Journal of Colloid and Interface Science 398 (2013) 67–73

Contents lists available at SciVerse ScienceDirect

Journal of Colloid and Interface Science

www.elsevier.com/locate/jcis

Microstructural changes of globules in calcium–silicate–hydrate gels with and without additives determined by small-angle neutron and X-ray scattering

Wei-Shan Chiang [a], Emiliano Fratini [b], Francesca Ridi [b], Sung-Hwan Lim [c], Yi-Qi Yeh [d], Piero Baglioni [b], Sung-Min Choi [c], U-Ser Jeng [d], Sow-Hsin Chen [a,*]

[a] Department of Nuclear Science and Engineering, Massachusetts Institute of Technology, Cambridge, MA, USA
[b] Department of Chemistry Ugo Schiff and CSGI, University of Florence, via della Lastruccia 3-Sesto Fiorentino, I-50019 Florence, Italy
[c] Department of Nuclear and Quantum Engineering, Korea Advanced Institute of Science and Technology, Daejeon, Republic of Korea
[d] National Synchrotron Radiation Research Center, Hsinchu Science Park, Hsinchu 30076, Taiwan

ARTICLE INFO

Article history:
Received 5 December 2012
Accepted 28 January 2013
Available online 18 February 2013

Keywords:
Calcium–silicate–hydrate
Portland cement
Polycarboxylic ether
Small-angle scattering
Colloid
Fractal structure

ABSTRACT

The microstructure of calcium–silicate–hydrate (C–S–H) gel, a major hydrated phase of Ordinary Portland Cement, with and without polycarboxylic ether (PCE) additives is investigated by combined analyses of small-angle X-ray scattering (SAXS) and small-angle neutron scattering (SANS) data. The results show that these comb-shaped polymers tend to increase the size of the disk-like globules but have little influence on the thickness of the water and calcium silicate layers within the globules. As a result, the fractal packing of the globules becomes more open in the range of a few hundred nanometers, in the sense that the mass fractal dimension diminishes, since the PCE adsorption on the globules increases the repulsive force between and polydispersity of the C–S–H units. Moreover, scanning electron microscope (SEM) study of the synthesized C–S–H gels in the micrometer range shows that the PCEs depress the formation of fibrils while enhancing the foil-like morphology.

1. Introduction

The mechanical properties of cement depend on the progressive maturation of hydrated porous phases due to the continuous reaction of water with the cement. This hydration process can last for several years. It is strongly affected by additives, many of which have been developed in recent years. The efficiency of these additives to produce high-performance concretes (HPC), that is, cement with extremely low porosity and enhanced strength and elasticity, is continuously being improved [1–3]. Superplasticizers (SPs) are compounds irreplaceable to the construction industry that are used as additives to produce HPC. These polymers have been shown to improve the flowability and workability of concrete pastes, to keep the water content of cement low, and to ensure the high mechanical strength, shrinkage, and durability of the hardened cementitious composite [1–3]. The comb-shaped polycarboxylic ethers (PCEs) are among the most effective SPs used in the cement industry. The simplest PCEs are composed of a polyacrylic or polymethacrylic anionic backbone with grafted polyethylene oxide (PEO) uncharged side chains. Each of these pieces can be tuned to produce several graft copolymers varying in the molecular weights and chemical structures. The effect of adding PCEs depends on the chosen chemical structure, which can dramatically alter the interaction between PCEs and the cement matrix [4–9]. The adsorption of the PCEs on the surface of the cement particles increases if the density or length of the PEO side chains is decreased. The decrease in side chain density increases the number of negative charges, that is, the number of free carboxylic groups on the backbone. Shortening of the PEO chain length not only reduces the overall steric hindrance, that is, rendering the negative charges on the backbone more accessible, but also increases the charge density of the entire polymer. Zingg et al. [10] studied the influence of PCEs on the microstructural evolution of the Portland cement during the early hydration stage. They concluded that surface charges of the silicate phases (i.e., tricalcium silicate (C_3S) and C–S–H) and aluminate phase (i.e., ettringite) depend on the ions present in the liquid phase (i.e., pore solution). PCEs adsorb on the surface of all the three phases but mainly on ettringite surface due to the direct adsorption of PCE on the ettringite particles. They suggested that PCEs adsorb indirectly on the Ca^{2+} counterion layer at the slip surface of C_3S and C–S–H through the interaction of the negative carboxylic groups on the PCE backbone with the positive calcium ions. Their results indicated that different levels of adsorption modify the rheology and hydration kinetics of the final cement pastes.

* Corresponding author. Fax: +1 617 258 8863.
E-mail addresses: weishanc@mit.edu (W.-S. Chiang), fratini@csgi.unifi.it (E. Fratini), ridi@csgi.unifi.it (F. Ridi), shlim11@kaist.ac.kr (S.-H. Lim), yeh.yq@nsrrc.org.tw (Y.-Q. Yeh), piero.baglioni@unifi.it (P. Baglioni), sungmin@kaist.ac.kr (S.-M. Choi), usjeng@nsrrc.org.tw (U-Ser Jeng), sowhsin@mit.edu (S.-H. Che).

0021-9797/$ - see front matter © 2013 Elsevier Inc. All rights reserved.
http://dx.doi.org/10.1016/j.jcis.2013.01.065

While the influence of PCEs on the macroscopic observables of cement (rheology, mechanical properties, and hydration dynamics) has been reported in the literature [4–9], the change in the C–S–H microstructure due to the PCE additives remains mostly unknown. Very recently, we used small-angle neutron scattering (SANS) to study the microstructure of synthesized pure calcium–silicate–hydrate (I) gel (C–S–H (I)) [11]. The analysis was based on Jennings' colloidal model-II (CM-II) [12,13]. In CM-II, C–S–H gel is described as a fractal-like object formed by the packing of colloidal particles called "globules". The globules are the basic building blocks of the C–S–H gel. Each globule has a lamellar sub-structure which was fully described by an appropriate form factor, allowing us to determine the evolution of the structural parameters in pure C–S–H (I) gel as a function of the water content [11]. The cartoons in Fig. 1a illustrate the intra-globule sub-structure and the inter-globule fractal structure. In this study, we use the combination of SANS and small-angle X-ray scattering (SAXS) techniques to investigate the microstructural changes of the C–S–H (I) gel before and after the addition of PCEs with defined chemical structures. Pure C–S–H gel together with four C–S–H gels including different PCEs, namely, PCE23-2, PCE23-6, PCE102-2, and PCE102-6, were studied [7]. To the best of our knowledge, this is the first time that the influence of PCE additives on the microstructure of C–S–H gel has been studied in detail.

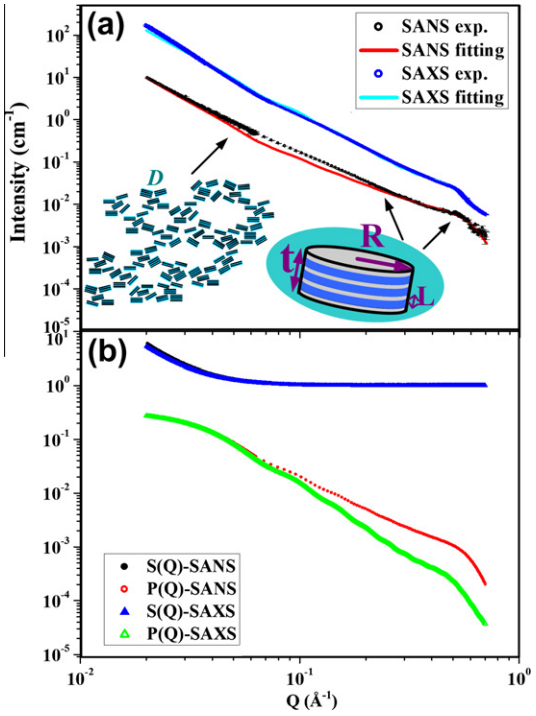

Fig. 1. Model fitting results of the pure C–S–H sample. (a) Experimental data of SAXS (blue open circle) and SANS (black open circle) and the corresponding data fitting curves of SAXS (cyan line) and SANS (red line) of the pure C–S–H sample. The SAXS experimental and fitting intensities are shifted in y-axis by timing a factor 10 for clarity. (b) inter-particle structure factor S(Q) of the SAXS data (blue solid triangle) and SANS data (black solid circle, not seen because it is almost the same curve as the S(Q) of the SAXS data) and intra-particle structure factor P(Q) of the SAXS data (green open triangle) and SANS data (red open circle) used to fit the data in panel (a). The difference in P(Q) comes from the different χ of neutron and X-ray. The error bars of the experimental data represent one standard deviation. The cartoons in panel (a) show the fractal structure suggested by S(Q) and the multi-layered cylinder model we use for P(Q). (For interpretation of the references to color in this figure legend, the reader is referred to the web version of this article.)

2. Materials and methods

2.1. Materials

Synthetic C–S–H was prepared by hydrating 4 g of pure tricalcium silicate (C_3S) in 1150 g of pure degassed water or 0.14% w/w PCE aqueous degassed solution (i.e., 0.4 g of polymer per 100 g of dry C_3S). All the water used in the synthesis was degassed to avoid any carbonation during the C_3S hydration. The chemically pure batch of C_3S (CTG-Italcementi, Bergamo) had a specific surface area of 0.65 m^2/g (BET). The molecular formulae of the four PCEs used in this study (i.e., PCE23-2, PCE23-6, PCE102-2, PCE102-6) are reported elsewhere along with relative polydispersities [7]. PCE23-2 and PCE23-6 have PEO side chains which are five times shorter than PCE102-2 and PCE102-6, while series 6 (i.e., PCE23-6 and PCE102-6) has more free carboxylic groups on the backbone. As a result, the adsorption ability results: PCE102-2 < PCE102-6 < PCE23-2 < PCE23-6. The hydration reaction was conducted at 25 °C for 40 days in sealed polyethylene bottles. The dispersions were filtered, and the water content was standardized by dehydrating the samples at 60 °C in a N_2 atmosphere. Final water content was about 20% as determined by thermogravimetric analysis on the so-obtained solids (operated at 10 °C/min. with a N_2 flux of 100 ml/min.). The sum of $Ca(OH)_2$ and $CaCO_3$ contents was always lower than 5% in all cases. Energy dispersive X-ray spectroscopy (EDS) evidenced an average Ca/Si ratio of about 1.6–1.9 in the cases of the pure C–S–H sample and PCEX-6 series, while in the case of PCEX-2 series, the ratio resulted slightly lower (1.3–1.5). Standard deviation is high in all cases (0.3–0.5) confirming the expected inhomogeneity of the sample. EDS spectra were recorded using a X-act microprobe (10 mm^2 silicon drift detector, Oxford Instruments) coupled with a SEM microscope (Carl Zeiss). Further specific details on the synthesis can be found elsewhere [11].

2.2. Methods

2.2.1. Small-angle neutron scattering (SANS) and small-angle X-ray scattering (SAXS)

SANS experiments were carried out at the High-Flux Advanced Neutron Application Reactor (HANARO) at Korea Atomic Energy Research Institute (KAERI), Daejeon, Republic of Korea. We used neutron wavelength, λ, of 5 Å and two configurations with sample-to-detector distances, SD, of 17.80 m and 1.16 m, respectively, to cover a wild Q-range of 0.002–0.909 $Å^{-1}$. SAXS measurements were conducted at the National Synchrotron Radiation Research Center (NSRRC), Hsinchu, Taiwan. Two sets of SD and λ, (4.94 m, 1.771 Å) and (1.18 m, 0.886 Å), were used to cover a Q-range parallel to the SANS measurements. The measurements were carried out at ambient temperature. Both SANS and SAXS data were rigorously corrected for electronic noise, sample transmission, background scattering and detector sensitivity, followed by a scaling to absolute intensity $I(Q)$ in cm^{-1} based on the scattering of a specific standard.

2.2.2. Thermogravimetry

Thermogravimetry was performed by means of a SDT Q600 (TA Instruments, Milan) from room temperature up to 900 °C, at a rate of 10 °C/min, under nitrogen flux (100 ml/min).

2.2.3. Scanning electron microscope (SEM) and energy dispersive X-ray spectroscopy (EDS)

Scanning electron microscope (SEM) investigations were performed on uncoated samples using a SIGMA field emission scanning microscope (Carl Zeiss Microscopy GmbH, Germany). The reported images were acquired using the In-Lens Secondary

Electron detector and working at a distance of about 3 mm with an acceleration potential of 2 kV. Energy dispersive X-ray spectroscopy (EDS) was performed by a 10 mm^2 silicon drift detector (X-Act) coupled with the SEM microscope and operated by the INCA software (Oxford Instruments). In this second case, the operative voltage of the electron source was raised to 5 kV and the working distance was increased to 8.5 mm to maximize the X-ray photon counts.

2.2.4. Analytical form of the small-angle scattering (SAS) model

In this work, we generalize the previously derived intensity formula used in the SANS data analysis [11] and apply it to the combined SAXS and SANS analysis. The combination of SANS and SAXS data analysis allows us to extract all the structural parameters much more accurately by introducing additional fitting conditions. The small-angle scattering (SAS) absolute intensity, in units of cm^{-1}, for a C–S–H gel consisting of globules immersed in the solvent (hydration water or air) can be expressed as:

$$I(Q) = N\langle\overline{P(Q)}\rangle_{Orientation,n}S(Q) + bg \ [cm^{-1}]. \tag{1}$$

N is a contrast prefactor. $S(Q)$ denotes the inter-globule structure factor of the porous C–S–H gel and $\langle\overline{P(Q)}\rangle_{Orientation,n}$ describes the normalized intra-particle structure factor averaged over the distribution of the number of layers (assumed to be a Schultz distribution) and all possible orientations of the globules. For SANS, $I(Q)$ in Eq. (1) should be further convoluted to the Q resolution function $R(Q)$, that is, $I(Q)_{Measure} = I(Q) \otimes R(Q)$ while for SAXS, dQ/Q is very small (<0.02) so for the first approximation, we neglect the Q resolution effect in the X-ray case.

In CM-II model, C–S–H gel consists of globules packing into a fractal-like object. The self-similar fractal structure is characterized by a fractal dimension D and a cutoff dimension of ξ. The gel is immersed in an aqueous solution or air depending on the water content [11]. Denoting the equivalent spherical radius of the globule as R_e, the inter-globule structure factor of the porous C–S–H gel can be calculated by [11].

$$\begin{aligned} S(Q) &= 1 + N_p\int_0^\infty dr\ 4\pi r^2\frac{\sin(Qr)}{Qr}g(r) \\ &= 1 + \frac{1}{(QR_e)^D}\frac{D\Gamma(D-1)\sin[(D-1)\tan^{-1}(Q\xi)]}{[1+(Q\xi)^{-2}]^{[(D-1)/2]}} \\ &= 1 + \left(\frac{\xi}{R_e}\right)^D\Gamma(D+1)\frac{\sin[(D-1)\tan^{-1}(Q\xi)]}{(D-1)[1+(Q\xi)^2]^{[(D-1)/2]}(Q\xi)} \end{aligned} \tag{2}$$

$\Gamma(x)$ in Eq. (2) is the gamma function.

In a previous study [11], the authors described a general mathematical form of the intra-particle structure factor $\overline{P(Q,\mu)}$, where $\mu = \cos\theta$. We assume the globules with sub-layered structure can have aspect ratio varying from cylinders to disks passing through spheroidal objects. In the following, we indicate the disk radius as R, the angle between $\vec{Q}$ and the globule rotation axis as θ, the layer thicknesses of hydration water and hydrated calcium silicate as L_1 and L_2, respectively, and their corresponding scattering length densities (SLDs) as ρ_1 and ρ_2, the interlayer distance as L, where $L = L_1 + L_2$, the solvent SLD as ρ_s, and the number of repeating layers inside a globule as n. Defining the normalized particle form factor as $\overline{F(Q,\mu)} = \frac{1}{\rho V_p}\int_{V_p}\rho(\vec{r})\exp(iQ\cdot\vec{r})d^3r$, where V_p is the volume of the globule, the normalized particle structure factor $\overline{F(Q,\mu)}$ is given by [11].

$$\overline{P(Q,\mu)} = |\overline{F(Q,\mu)}|^2 = \left[\frac{2J_1(QR\sqrt{1-\mu^2})}{QR\sqrt{1-\mu^2}}\right]^2 C^2(A^2+B^2), \tag{3}$$

where

$$A = \chi\cos\left(\frac{Q\mu(nL-L_2)}{2}\right)\frac{\sin\left(\frac{Q\mu L_1}{2}\right)}{Q\mu} + \cos\left(\frac{Q\mu(nL+L_1)}{2}\right)\frac{\sin\left(\frac{Q\mu L_2}{2}\right)}{Q\mu},$$

$$B = \chi\sin\left(\frac{Q\mu(nL-L_2)}{2}\right)\frac{\sin\left(\frac{Q\mu L_1}{2}\right)}{Q\mu} + \sin\left(\frac{Q\mu(nL+L_1)}{2}\right)\frac{\sin\left(\frac{Q\mu L_2}{2}\right)}{Q\mu},$$

$$C = \frac{2}{n[\chi L_1 + L_2]}\frac{\sin\left(\frac{Q\mu nL}{2}\right)}{\sin\left(\frac{Q\mu L}{2}\right)} \text{ and } \chi = \frac{\rho_1-\rho_s}{\rho_2-\rho_s}.$$

The particle structure factor $\overline{P(Q,\mu)}$ should be averaged over all possible axis directions by $\langle\overline{P(Q)}\rangle_{Orientation} = \int_0^1\overline{P(Q,\mu)}d\mu$. Moreover, we should expect that the number of layers n, the cylindrical globule radius R, and the interlamellar distance L all have their own distributions. However, here we only introduce an "effective" distribution for the number of layers $f_S(n)$ to take into account all the possible contributions. We assume the effective polydispersity to be a Schultz distribution given by:

$$f_S(n) = \left(\frac{Z+1}{\bar{n}}\right)^{Z+1}n^Z\exp\left[-\left(\frac{Z+1}{\bar{n}}\right)n\right]/\Gamma(z+1) \quad Z > -1, \tag{4}$$

where $\bar{n}$ is the mean of the distribution, Z is a width parameter, and $\Gamma(x)$ is the gamma function. The standard deviation of $f_S(n)$ can be calculated by $\sigma_n = (\bar{n^2} - \bar{n}^2)^{1/2} = \bar{n}/(Z+1)^{1/2}$.

Therefore, the final form of the normalized average particle structure factor can be obtained by:

$$\langle\overline{P(Q)}\rangle_{Orientation,n} = \int_0^\infty\langle\overline{P(Q,n)}\rangle_{Orientation}f_S(n)dn.$$

The important parameters contained in the intra-particle structure factor in Eq. (3) are R, L_1, L_2, $L = L_1 + L_2$, χ, $\bar{n}$, and Z. The parameters contained in the inter-globular structure factor in Eq. (2) are D and ξ. The equivalent radius R_e of a globule can be calculated as $R_e = (3\bar{n}R^2L/4)^{(1/3)}$. Ideally, the difference between the SANS and SAXS models only occurs in the factor χ, that is, χ_{SANS} and χ_{SAXS}, the prefactor N, that is, N_{SANS} and N_{SAXS}, and the constant background, that is, bg_{SANS} and bg_{SAXS}.

3. Results and discussion

We first conducted non-linear least square fitting to SAXS data and used the resulting parameters as known parameters to input into the SANS model, allowing only N_{SANS}, χ_{SANS}, and bg_{SANS} to change. We fixed χ_{SAXS} to be 0.064 for both C–S–H gels with and without additives, assuming the density of the calcium silicate layer to be the same as that of the C–S–H particle in D-drying condition [12]. This is reasonable because the scattering length densities of PCEs are very close to water's SLD. Ideally, L_{SANS} and L_{SAXS} should be the same, but we allowed this parameter to relax a few angstroms, considering the different resolutions of the two instruments. Also, we only fitted the Q-range of 0.02 $Å^{-1}$ < Q < 0.70 $Å^{-1}$ and neglected the surface fractal effect in the Q-range chosen for the SAXS and SANS data analysis. This is because the surface fractal feature is mainly present within the Q-range below 0.01 $Å^{-1}$ [12,13]. Finally, because the change of the ξ during the fitting process had little effect on the inter-particle structure factor $S(Q)$ in the range of Q > 0.02 Å, we fixed ξ at 670 Å in accordance with what is reported in Refs. [11,12].

Fig. 1 shows the SAXS and SANS data fitting of pure C–S–H gel measured at 25 °C together with their corresponding $S(Q)$ and $P(Q)$. The difference between the SAXS and SANS intensities comes from the different SLDs of X-ray and neutron, which contribute to $P(Q)$. The cartoons in Fig. 1a show the inter-globule fractal structure (pointed by the arrow to low Q) and the intra-globule sub-structure (pointed by the arrows to high Q). The comparison of SANS and SAXS data fitting results for all of the samples is shown in Fig. 2. The model we used agrees with both SANS and SAXS data over the wide Q-range from 0.02 $Å^{-1}$ to 0.70 $Å^{-1}$. The fitting parameters used in Figs. 1 and 2 are listed in Table 1.

The thickness of calcium silicate layer L_2 obtained from the SAXS data fitting is close to the result of grand canonical Monte Carlo (GCMC) simulation (3.3–3.9 Å) [14,15] and what was found in the previous SANS study (3.47 Å) [11]. The results here show that the thicknesses of both the water layer (L_1) and the calcium silicate layer (L_2) do not change much when PCEs are added, indicating that PCEs do not form any intercalation products with this phase unlike the case of Al-rich hydrates, that is, the AFm phase [16]. However, the additives enlarge the C–S–H globules in two ways. First, the average number of repeating layers $\bar{n}$ increases for all of the samples with additives, suggesting that PCEs are able to bind more layers together. Second, the globule disk radius R increases in samples with additives of PCE23-2 and PCE102-6. This means that when adding PCE23-2 and PCE102-6, the microstructure of C–S–H becomes more like the continuous extension of branched or interconnected multi-lamellar sheets, as in the models proposed by Dolado et al. [17,18] and McDonald et al. [19]. In addition, by fitting the SAXS data with $I(Q) = C_p \times Q^{-4}$ in the range of 0.23 $Å^{-1} < Q < 0.29$ $Å^{-1}$, where the contribution from $S(Q)$ is negligible, we found that the Porod constant C_p (not shown), which is proportional to the total surface area per volume, has the trend: C–S–H > C–S–H/PCE102-2 > C–S–H/PCE23-6 > C–S–H/PCE23-2 > C–S–H/PCE102-6. This trend is inverse to the trend of the effective radius R_e of the globules (see Table 1) except for PCE23-2 and PCE102-6. This is reasonable because particles with larger radius have smaller specific surface area. Surprisingly, the globules pack into a more open fractal structure when additives are present, as shown by the decrease in fractal dimension D (see Table 1). Uchikawa et al. [20] conducted atomic force microscope (AFM) measurements on Ordinary Portland Cement with and without PCE and found that the addition of PCE significantly increases the intensity and range of the steric repulsive force introduced by the additives. Ferrari et al. [21] investigated the interaction of PCE23-6 with model surfaces using AFM, adsorption isotherms, and zeta potential. The main tendency for PCEs in cement is to adsorb on positively charged surface in order to avoid positive–negative particle aggregation. When particles do not adsorb SPs, the electrostatic interaction dominates, otherwise the steric repulsion dominates. The enhanced dispersion forces can explain the more open structure in the case of C–S–H (I) pastes containing PCEs, where the particles all have the same charge as a result of the simplicity of the synthetic phase which is almost free of $Ca(OH)_2$. The more open structure can be also due to the more disperse number of layers in the samples containing PCEs compared with the pure C–S–H (I) sample. This can be seen clearly in Fig. 3, which shows the effective Schultz distribution of the total thickness of the globules ($t = nL$), contributed from the effective distribution of the number of repeating layers, for all the investigated cases. The high polydispersity of the globules in the samples with PCEs makes the globules hard to pack into a compact structure. This is consistent with the authors' previous study [11], in which we showed that C–S–H gel with lower water content has a higher fractal dimension (a more compact fractal structure) and a more uniform distribution with respect to the number of layers. Finally, we estimated the number density of the globules N_P (not shown) through the prefactor $N = N_P(\Delta\rho V_p)^2$ and found that N_P has the trend C–S–H > C–S–H/PCE102-2 > C–S–H/PCE23-6 > C–S–H/PCE102-6 > C–S–H/PCE23-2 (i.e., the reverse of the particle size trend). This is expected because with the same amount of C_3S, the gel with larger globule size should have lower globule number density. The lower N_P can also explain the more open fractal structure formed by the samples in the presence of additives.

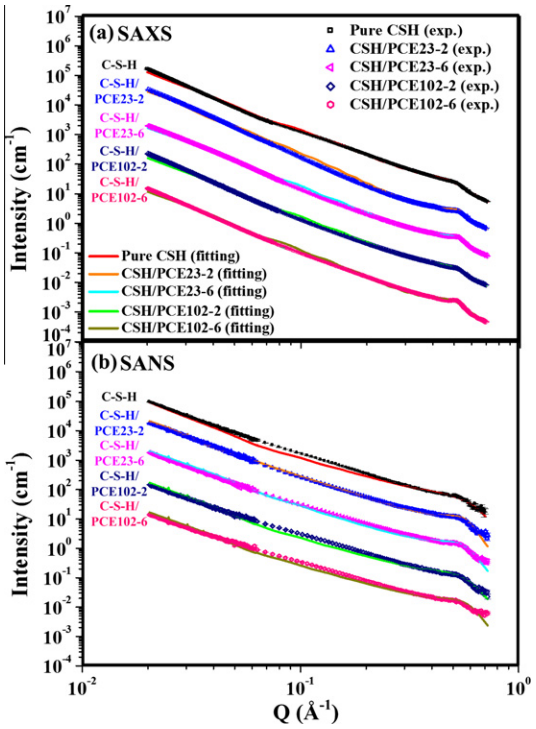

Fig. 2. Model fitting results of (a) SAXS data and (b) SANS data. Both panels show the experimental data for pure C–S–H (black open square), C–S–H/PCE23-2 (blue open up-triangle), C–S–H/PCE23-6 (magenta open left-triangle), C–S–H/PCE102-2 (navy open diamond), C–S–H/PCE102-6 (pink open hexagon), and the data fitting curves for pure C–S–H (red), C–S–H/PCE23-2 (orange), C–S–H/PCE23-6 (cyan), C–S–H/PCE102-2 (green), C–S–H/PCE102-6 (dark yellow). The experimental and fitting intensities are shifted in y-axis by timing factors of 10^4 (pure C–S–H), 10^3 (C–S–H/PCE23-2), 10^2 (C–S–H/PCE102-6), and 10^1 (C–S–H/PCE102-2) for clarity. (For interpretation of the references to color in this figure legend, the reader is referred to the web version of this article.)

The thermogravimetric analysis performed on the pastes containing PCEs is shown in Fig. 4 as derivative weight loss signal versus temperature. A well-defined peak due to the polymer decomposition is evident at around 400 °C for the C–S–H/PCE102-6 and C–S–H/PCE23-6 samples. For the cases of CSH/PCE102-2 and CSH/PCE23-2, this peak is barely distinguishable from the base line. A second feature is shown at about 380 °C in almost all cases. The estimated mass losses due to the presence of adsorbed polymers (considered the baseline due to the degradation of the inorganic phase) are 0.4 ± 0.1% for C–S–H/PCE102-6 and C–S–H/PCE23-6 and 0.2 ± 0.1% for C–S–H/PCE102-2 and C–S–H/PCE23-2. These semi-quantitative observations are in agreement with the literature [4–10], confirming the higher propensity of the PCEX-6 series to be adsorbed on the calcium silicate phase, as a result of the higher amount of charged carboxylic groups present on the backbone.

Ridi et al. [7] previously studied the hydration reaction of tricalcium silicate (C_3S) in the presence of the same four PCEs investigated in this study. Their results showed that decreasing PEO side chain length and density increases the induction time. As a result, the induction time followed the sequence of C_3S/PCE23-

Table 1
Parameters extracted from the model fitting of SAXS and SANS data.[a]

Sample	L_{SAXS} (Å)	L_2 (Å)	$\bar{n}$	R (Å)	D	R_e (Å)	L_{SANS} (Å)	χ_{SANS}
CSH	13.05(3)	4.46(5)	0.85(1)	59.31(8)	2.81(1)	30.81(9)	10.7(2)	-0.25(2)
CSH + PCE23-2	12.06(1)	4.4(1)	2.46(1)	104.1(1)	1.67(1)	62.23(9)	11.22(3)	-0.31(1)
CSH + PCE23-6	12.36(1)	4.80(4)	1.48(1)	59.08(8)	2.62(1)	36.28(9)	11.33(4)	-0.27(1)
CSH + PCE102-2	12.76(3)	4.20(7)	1.01(1)	58.92(8)	2.70(1)	32.3(1)	11.23(7)	-0.23(1)
CSH + PCE102-6	12.54(1)	4.46(5)	1.48(1)	66.7(1)	2.68(1)	39.6(2)	10.93(4)	-0.32(1)

[a] ξ is fixed as 670 Å [11,12] and χ_{saxs} is fixed as 0.064, assuming the density of the calcium silicate layer to be the same as C–S–H particle in D-drying condition. The width parameter Z of the number of layers with Schultz distribution is collapsed onto the lowest boundary 0.01 set by the fitting process, indicating the wide distribution of n. Here, we allow L_{SAXS} and L_{SANS} to be different within a few angstroms to consider the difference of the instrument resolutions.

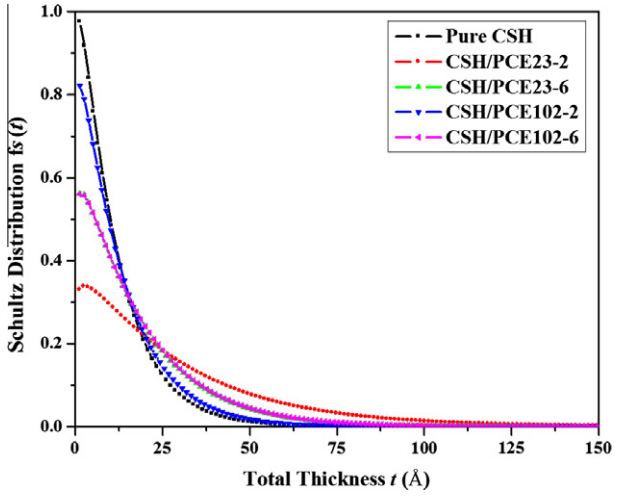

Fig. 3. The effective Schultz distribution of the total thickness $t = nL$ of the globules for samples of pure C–S–H (black line with solid square), C–S–H/PCE23-2 (red line with solid circle), C–S–H/PCE23-6 (green line with solid up-triangle), C–S–H/PCE102-2 (blue line with solid down-triangle), and C–S–H/PCE102-6 (magenta line with solid left-triangle). The normalization condition is $\int_0^\infty f_S(t)\,dt = L$ (For interpretation of the references to color in this figure legend, the reader is referred to the web version of this article.).

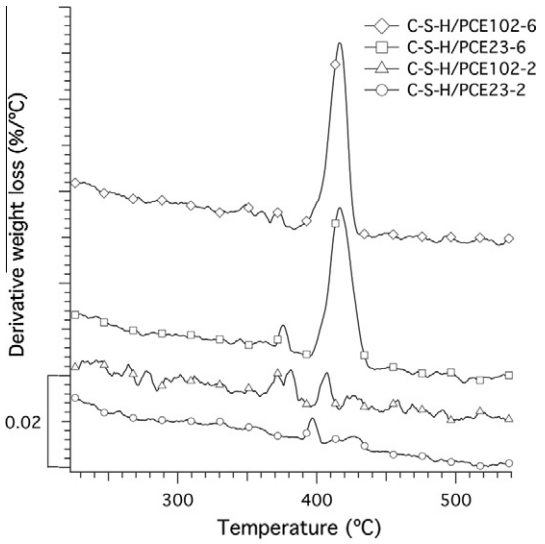

Fig. 4. Detail of the thermogravimetric measurements, presented as derivative weight loss versus temperature, of the four C–S–H samples synthesized in presence of additives. The pure C–S–H sample (not shown here) gives a smooth baseline showing no features in the reported temperature range and in particular at 380 and 400 °C.

6 > C_3S/PCE23-2 > C_3S/PCE102-6 > C_3S/PCE102-2 > pure C_3S. The results here indicate that for the longer PEO chain cases, that is, PCE102-Y series, the PCE with lower side chain density (PCE102-6) induces globules with a larger disk radius and a large average number of layers. These globules pack into a more open fractal structure compared with the higher side chain density sample (PCE102-2) and the pure C–S–H sample. This should be related to the fact that a PCE with a lower side chain density has a higher adsorption on the C_3S starting powder as well as on the final C–S–H particles and hence affects more on the microstructure of C–S–H [4–10]. However, surprisingly, the PCE23-Y series (shorter PEO chain length) shows the reverse trend. The higher chain density polymer (PCE23-2) induces the greatest change in the C–S–H microstructure. Actually, C–S–H/PCE23-2 has parameters very different from the parameters of other samples (see Table 1) and the reason for this is not clear yet. A field emission scanning electron microscope (FE-SEM) investigation was conducted to clarify this point. The FE-SEM images displayed in Fig. 5 shows that in the pure C–S–H sample (panels (a) and (b)), two different morphologies are present: zones of fibrillar structures and areas with networks of foils coexisting all over the sample. Working at a very high w/c ratio results in a very inhomogeneous sample with respect to the morphology and the composition, as testified both by SEM images and EDS analysis, which shows the broad range of Ca/Si ratio ranging from 1.6 to 2.0. On the other hand, almost no sign of fibril is found in the samples containing additives (panels (c)–(j)), where the main morphology consists of flat structures arranged in sponge-like networks. If we consider these sponge-like features closely, it is clear that a more compact structure is achieved when the PCEs are present in the pastes, which is consistent with the expectation that PCEs produce high-performance concretes with low porosity. Moreover, it can be observed that in the cases of PCE23-2, PCE23-6 and PCE102-6, the global morphology is more amorphous and compact than the other cases. At this stage, we have to remember that SEM and SAS techniques give complementary information and pertain different dimensional ranges, rendering difficulty to reconcile the results. An ultra-SAS experiment would allow us to link the extracted fractal dimensions to the actual morphology in the micrometer dimensional range.

4. Conclusions

We studied the effect of adding PCEs with controlled molecular architectures on the microstructure and nanostructure of the synthesized C–S–H (I) gel and its globules using the combination of SAXS and SANS techniques. The combined data analysis gives additional fitting conditions to extract the structural parameters accurately. We demonstrated, for the first time, that PCE additives can enhance the local stacking of the calcium silicate sheets through increasing the average number of repeating layers in the globules, which further pack into more open fractal-like structures in the range of a few hundred nanometers. The layer thickness of a globule is not significantly affected by the PCEs added. This is a clear proof of the lack of any intercalation phenomena in the C–S–H/

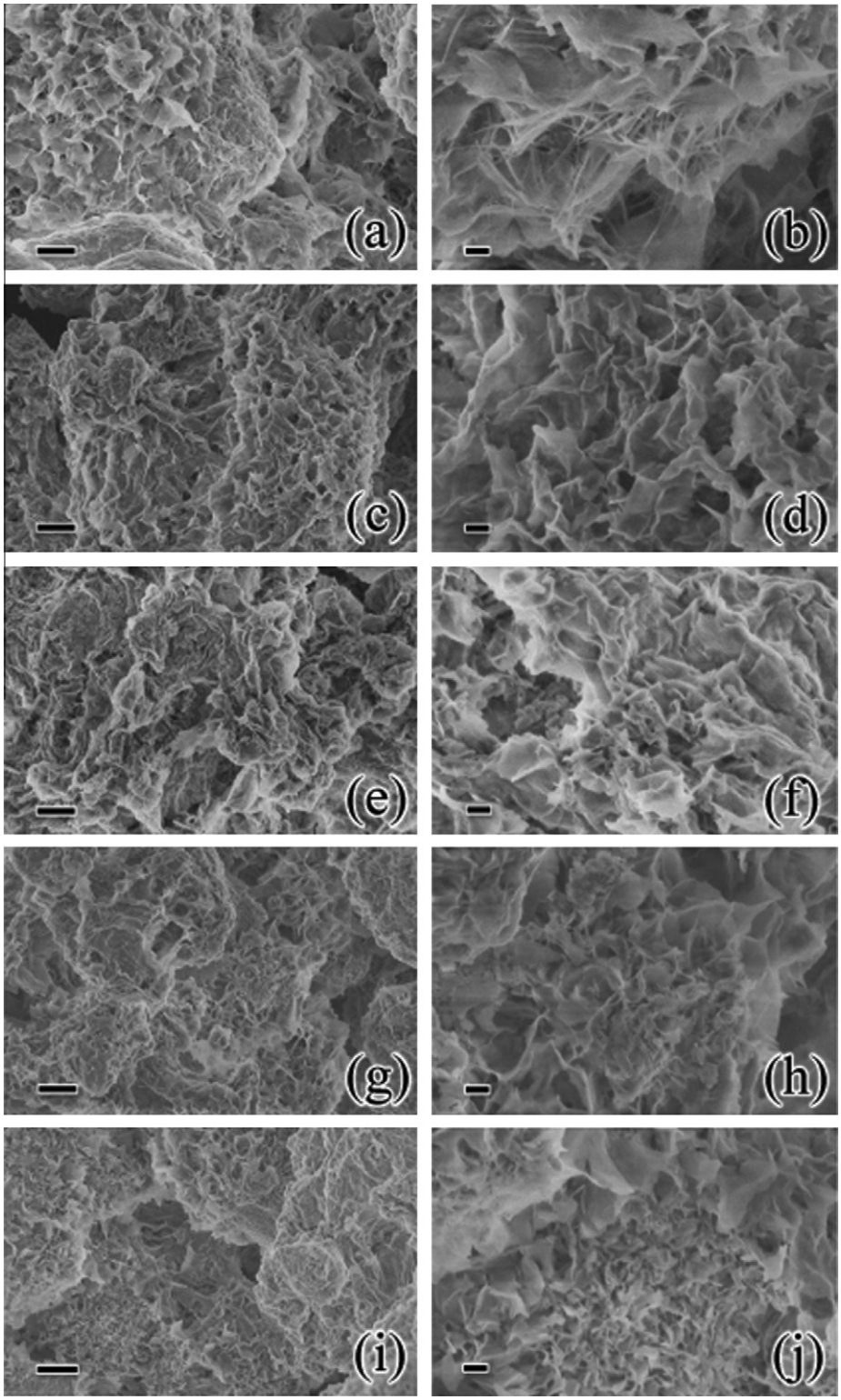

Fig. 5. FE-SEM images of (a) and (b) C–S–H, (c) and (d) C–S–H/PCE102-2, (e) and (f) C–S–H/PCE102-6, (g) and (h) C–S–H/PCE23-2, and (i) and (j) C–S–H/PCE23-6. Images on the left correspond to 25× magnification (bar = 1 μm) while images on the right correspond to 75× magnification (bar = 200 nm).

PCE systems, in contrast to what is usually found in Al-rich phases. The investigation in the micrometer range evidences that the PCEs depress the fibril formation characteristic of the C–S–H (I) phase in favor of a foil-like morphology, which is more compact and interconnected. The pastes containing PCE23-6, PCE102-6 and PCE23-2, which have higher adsorption propensity toward the calcium silicate phase, result more abundant in amorphous regions, showing less extended foils. These findings are fundamental for understanding the effect of superplasticizers at a microscopic level. In the future, this enhanced understanding could allow a fine tun-

ing of the structure and mechanical properties of C–S–H, and in turn those of cement.

Acknowledgments

This research is supported by DOE grant number DE-FG02-90ER45429. We kindly thank CTG-Italcementi for providing the C_3S pure phase and for partial financial support. Dr. S. Becker and Dr. J. Pakusch (BASF AG) are acknowledged for providing the PCEs. EF, FR, and PB thank partial financial support from MIUR and CSGI. SHL and SMC thank partial financial support from NRF/MEST (No. 2011-0031931), HANARO, KAERI and Dr. T.-H. Kim is acknowledged for providing SANS beamtime and technical support during experiment, respectively. Dr. C. Bertrand is acknowledged for reading and correcting the manuscript.

References

[1] F. Ridi, E. Fratini, P. Baglioni, J. Colloid Interface Sci. 357 (2011) 255.
[2] C. Jolicoeur, M.A. Simard, Cem. Concr. Compos. 20 (1998) 87.
[3] E. Sakai, M. Daimon, Mater. Sci. Concr. 4 (1995) 91.
[4] W. Prince, A. Espagne, P.C. Aitcin, Cem. Concr. Res. 33 (2003) 635.
[5] F. Winnefeld, S. Becker, J. Pakusch, T. Goetz, Cem. Concr. Compos. 29 (2007) 251.
[6] K. Yamada, T. Takahashi, S. Hanehara, M. Matsuhisa, Cem. Concr. Res. 30 (2000) 197.
[7] F. Ridi, E. Fratini, P. Luciani, F. Winnefeld, P. Baglioni, J. Phys. Chem. C 116 (2012) 10887.
[8] G.H. Kirby, J.A. Lewis, J. Am. Ceram. Soc. 87 (2004) 1643.
[9] C.Z. Li, N.Q. Feng, Y.D. Li, R.J. Chen, Cem. Concr. Res. 35 (2005) 867.
[10] A. Zingg, F. Winnefeld, L. Holzer, J. Pakusch, S. Becker, L. Gauckler, J. Colloid Interface Sci. 323 (2008) 301.
[11] W.S. Chiang, E. Fratini, P. Baglioni, D. Liu, S.H. Chen, J. Phys. Chem. C 116 (2012) 5055.
[12] A.J. Allen, J.J. Thomas, H.M. Jennings, Nat. Mater. 6 (2007) 311.
[13] H.M. Jennings, Cem. Concr. Res. 38 (2008) 275.
[14] R.J.M. Pellenq, A. Kushima, R. Shahsavari, K.J. Van Vliet, M.J. Buehler, S. Yip, F.J. Ulm, Proc. Natl. Acad. Sci. 106 (2009) 16102.
[15] M. Youssef, R.J.M. Pellenq, B. Yildiz, J. Am. Chem. Soc. 133 (2011) 2499.
[16] C. Giraudeau, J.B. d'Espinose de Lacaillerie, Z. Souguir, A. Nonat, R.J. Flatt, J. Am. Ceram. Soc. 92 (2009) 2471.
[17] J.S. Dolado, M. Griebel, J. Hamaekers, J. Am. Ceram. Soc. 90 (2007) 3938.
[18] J.S. Dolado, M. Griebel, J. Hamaekers, F. Heber, J. Mater. Chem. 21 (2011) 4445.
[19] P.J. McDonald, V. Rodin, A. Valori, Cem. Concr. Res. 40 (2010) 1656.
[20] H. Uchikawa, S. Hanehara, D. Sawaki, Cem. Concr. Res. 27 (1997) 37.
[21] L. Ferrari, J. Kaufmann, F. Winnefeld, J. Plank, J. Colloid Interface Sci. 347 (2010) 15.